Bulletin of Engineering Geology and the Environment (2021) 80:9029–9047
https://doi.org/10.1007/s10064-021-02479-w

ORIGINAL PAPER

Ground vibration characteristics of carbon dioxide phase transition fracturing: an in situ test

Shengtao Zhou[1] · Xuedong Luo[1,2] · Nan Jiang[1,2] · Shitong Zhang[1] · Yu Lei[1]

Received: 22 January 2021 / Accepted: 20 October 2021 / Published online: 4 November 2021

Abstract

Carbon dioxide phase transition fracturing is a safe rock-breaking technique. Its vibration effect cannot be ignored. It is valuable for fracturing safety control to investigate its ground vibration characteristics. In this paper, a single-hole test was implemented, and several vibration curves in jet direction and vertical jet direction were monitored to explore the ground vibration difference in these two directions. The attenuation laws of the peak particle velocity (PPV) and the Fourier dominant frequency were obtained. Moreover, based on the Hilbert–Huang transform method, the time–frequency–energy characteristics for the fracturing vibration were evaluated. The test results indicated that the PPV in jet direction is higher than that of the vertical jet direction, and the PPV obeys the power attenuation function in these two monitoring directions. When the explosion center distance increases from 2.193 to 6.067 m, the Fourier dominant frequency fluctuates slightly around 2 Hz in jet direction, but it decays from 12.5 to 1.6 Hz in the vertical jet direction. The vibration signal energies in jet direction and vertical jet direction are both distributed within 0–48 Hz. In addition, it is indicated that the vibration signal energy converses from a high-frequency band to a low-frequency band as the explosion center distance rises from 2.193 to 6.067 m. Due to the significant difference between the ground vibrations in the diverse directions, when this fracturing technique is carried out near the buildings, it is suggested that the installation direction of the fracturing pipe should be considered.

Keywords Carbon dioxide phase transition fracturing · Peak particle velocity · Dominant frequency · Hilbert–Huang transform · Energy distribution

Nomenclature

v_1	Peak particle velocity for the jet direction (cm/s)
r	Explosion center distance (m)
R^2	Coefficient of determination
v_2	Peak particle velocity for the vertical jet direction (cm/s)
f_{vd}	Fourier dominant frequency in vertical jet direction (Hz)
$v(t)$	Original non-stationary signal
$h_i(t)$	ith intrinsic mode function component
$r(t)$	Signal residual
P_E	Energy proportion of 0–20 Hz in jet direction (%)

✉ Nan Jiang
happyjohn@foxmail.com

Shengtao Zhou
stzhou@cug.edu.cn

Xuedong Luo
cugluoxd@foxmail.com

Shitong Zhang
stzhang@cug.edu.cn

Yu Lei
cugleiyu@cug.edu.cn

[1] Faculty of Engineering, China University of Geosciences, Wuhan, China

[2] Hubei Key Laboratory of Blasting Engineering, Jianghan University, Wuhan, China

Introduction

Blasting is often not allowed in rock excavation projects around sensitive areas such as schools and hospitals, since it usually causes adverse effects such as vibration, overpressure, and flying stones (Ozer 2008; Xu et al. 2017; Jiang et al. 2020). As an alternative technique for blasting, the carbon dioxide phase transition fracturing has several advantages including high excavation efficiency, low noise, no sparks, and no high-temperature gas, which provides a novel rock excavation method in serious environments (Kang et al. 2018; Chen et al. 2019; Li et al. 2020).

Carbon dioxide phase transition fracturing (CDPTF) was invented in the last century. To reduce blasting risks, it was mainly utilized as a substitute for explosives to excavate coal seams. As time passes by, it was gradually discontinued due to the mature application of mine machinery (Weir and Edwards 1928; Clairet 1952; Wilson 1954; Hawkes 1958; Lu et al. 2015; Ke et al. 2019a; Yang et al. 2019c). In recent years, the ascendancies of CDPTF in improving gas drainage and excavation safety have regained a lot of attention. Therefore, this technique has been reused in gas drainage, mining, municipal engineering, and pipeline cleaning (Miller 1995; Zou and Panawalage 2001; Pantovic et al. 2002; Vidanovic et al. 2011; Zhang et al. 2013; Zhang et al. 2015; Lu et al. 2015; Ke et al. 2019a; Hu et al. 2019). The energy difference of carbon dioxide in different phases is utilized as the rock-breaking power; thereby, this technique is regarded as a physical explosion technique (Patrick 1995; Caldwell 2005; Chen et al. 2017a). Besides, since the liquid carbon dioxide used in this technique is an inert substance with excellent stability, the transportation process is safe and reliable; no government approval is required when conducting the carbon dioxide phase transition fracturing (Chen et al. 2019; Yang et al. 2019a).

Over the past few years, scholars show an increasing interest in the fracturing load, rock fracture mechanism, and pore structure damage of rock mass subjected to the CDPTF. Identifying the fracturing load characteristics is the first step to develop the fracturing theory for CDPTF. With the reference to the calculation method for pressure vessels' explosion energy, Dong et al. (2014) introduced the TNT equivalent calculation method to describe the total fracturing energy. Guo et al. (2018) and Ke et al. (2019a) based on the Span and Wagner equation of state, proposed a more accurate fracturing energy calculation method. As an external manifestation of the energy, the ground vibration can also reflect the total fracturing energy of the explosion. Yang et al. (2019a) calculated the TNT equivalent of CDPTF by comparing the root mean square of the ground vibration excited by the TNT and CDPTF. In addition, the rock fracture mechanism under the above fracturing load is also a key issue. Singh (1998) believed that the pressure exerted by the high-pressure gas created a tensile stress field inside the rock mass, and the rock failed by tensile stress, and then a cone-shaped crack was formed inside the rock mass. Gao et al. (2018) thought that the gas wedge also played an important role in rock fracture, and indicated that the gas pressure is only applied to the part of the area on the drill hole, the radial displacement caused by the compressive stress led to the formation of the tensile stress field in the rock, initial tensile cracks appeared first in the vertical jet direction on the borehole under the condition of no confining pressure, and then they propagated again under the gas wedge. Zhang et al. (2018, 2019) investigated the rock fracture characteristics by conducting the CDPTF test on the free-field concrete, and the peridynamic simulations were taken to evaluate rock fracture, drawing the conclusion that the rock fragmentation was controlled by the combined effect of jet impact and the gas wedge of high-pressure carbon dioxide. Rock fragmentation is an intuitive effect of CDPTF. In fact, in the unbroken surrounding rock, the fracturing impact causes rock damage, which is the internal manifestation of the fracturing effect. This damage is usually defined through the pore structure statistical parameters of the rock. Aimed at this issue, based on the scanning electron microscope and the mercury intrusion method, Liu et al. (2020) observed many microfractures and macropore clusters after fracturing and found that the pore connectivity of coal was improved. As mentioned above, this fracturing technique cannot only induce the generation of macroscopic cracks but also cause damage to the microstructure of the rock, so it was regarded as a good method to enhance the permeability of coal seams. Many scholars (Lu et al. 2015; Chen et al. 2017a, b; Cao et al. 2017; Kang et al. 2018; He et al. 2018; Yang et al. 2019b) applied the CDPTF in the coal mines to enhance permeability; all the results indicated that the permeability of the coal seam is significantly improved after the fracturing treatment.

Despite the loading rate for CDPTF is much less than that of blasting, the fracturing drill hole is subjected to the rapid impact of high-pressure gas during the fracturing process, which inevitably leads to vibration of the surrounding rock. Due to the huge difference in the proportion of stress wave and high-pressure gas energy, the vibration aroused by high-pressure CO_2 fracturing and blasting is also dissimilar. The shock wave intensity for this physical explosion technique is low, and the peak particle velocity of CDPTF is correspondingly small. However, it is worth noting that the dominant frequency corresponding to this vibration is also low. As we all know, low-frequency vibration can easily cause resonance of engineering structures; this vibration may bring greater risks to the surrounding buildings (Zeng et al. 2020). Therefore, it is important for safety control to investigate the ground vibration for CDPTF. More and more scholars have paid more attention to the vibration characteristics of CDPTF. Based on the wavelet packet transform, Chen et al. (2018) studied the fracturing vibration signals in bench rock breaking with five fracturing pipes, which indicated that the dominant frequency is among the 0–4 Hz sub-band. Liu et al. (2018) analyzed the frequency spectrum and energy distribution characteristics of the fracturing signals with three fracturing pipes being detonated at the same time and found that the vibration frequency was mainly in the range of 0 ~ 100 Hz and the energy was mainly concentrated in 0 ~ 0.5 s. Ke et al. (2017) monitored the seismic waves of CDPTF at a distance of 12 m from the explosion center

and analyzed the collected signals through the adaptive optimal kernel time–frequency analysis method, drawing the conclusions that there was no obvious S wave in the vibration signals, and the vibration energy was mainly distributed in 0 ~ 125 Hz. Zeng et al. (2020) analyzed the multiple drill holes fracturing vibration signals through frequency slice wavelet transform (FSWT) and found that the main frequency band was 4.4 ~ 63.7 Hz, and the vibration energy within 0 ~ 20 Hz accounted for 92.9% of the total energy. After six fracturing pipes were detonated at the same time, Li et al. (2020) investigated the fracturing vibration signals near the reinforcement wall through the discrete Fourier transform and found that 85% of energy was distributed in 6–60 Hz, and the signal energy attenuated faster but distributed tighter with the increase of distance.

Prior studies about carbon dioxide phase transition fracturing vibration have conducted preliminary investigations on the fracturing vibration signals. However, when monitoring the fracturing vibration curves, most of the existing tests did not consider the positional relationship between the energy release port and the layout direction of the monitoring point. It is generally acknowledged that the fracturing pipe widely used in rock excavation has a special mechanical structure, high-pressure carbon dioxide is released along the preset channel, and thus, the borehole wall facing the gas outlet received a greater impact, which caused the gathering energy effect. Previously published studies have recognized that the critical role played in the fracturing process by the gathering energy effect, and the vibration characteristics in different directions are discrepant (Guo 2017; Zhou et al. 2020). What is not yet clear is the impact of the gathering energy effect on the vibration in different directions.

In this paper, we took the gathering energy effect into consideration, firstly carried out a single-hole carbon dioxide phase transition fracturing in situ test, and monitored several velocity–time curves in the two directions (i.e., jet direction, vertical jet direction). Furthermore, the Hilbert–Huang transform was chosen to analyze the time–frequency characteristics and energy distribution of the vibration signal. It is expected that the research results in this study would lay the groundwork for subsequent research into the establishment of fracturing vibration safety criteria and the safety control for its harmful effects.

Principle of carbon dioxide phase transition fracturing

The fracturing pipe is the essential piece of equipment in CDPTF, which is composed of a filling head, a liquid CO_2 storage pipe, a discharge head, a shear sheet, a heating tube, and two sealing gaskets. The mechanical structure of it is shown in Fig. 1.

Among them, the filling head, the liquid CO_2 storage pipe, and the discharge head are made of 42CrMo which undergoes thermal refining, and the thickness of the storage pipe meets the analytical solution for the thick-walled cylinder. The shear sheet determines the peak inner pressure of the fracturing pipe, which is the key component to affect the total fracturing energy. As can be seen from Fig. 1, the heating tube is set in the CO_2 storage pipe. When the fracturing is carried out, it would be initiated by the little electric current and generate a large amount of heat instantly, prompting the rapid phase transition of liquid carbon dioxide into the supercritical state. Besides, the two symmetrical energy release ports are set on the discharge head, which are the release channels for the high-pressure carbon dioxide (Singh 1998; Ke et al. 2019b). To fill the liquid carbon dioxide into the fracturing pipe, the filling equipment is also needed. As shown in Fig. 2, the filling equipment includes a dewar, a tightening machine, a filling machine, and a filling shelf.

When carrying out the carbon dioxide phase transition fracturing, we should assemble the whole parts of the fracturing pipe through the tightening machine firstly, then the filling machine is applied to fill the liquid carbon dioxide into the CO_2 storage pipe. It should be noted that before liquid carbon dioxide is filled into the CO_2 storage pipe, it all was stored in the dewar. Latterly, the filled fracturing pipe is subsequently pushed into the drill hole, and the drill hole was blocked. When all the preparations are completed, the

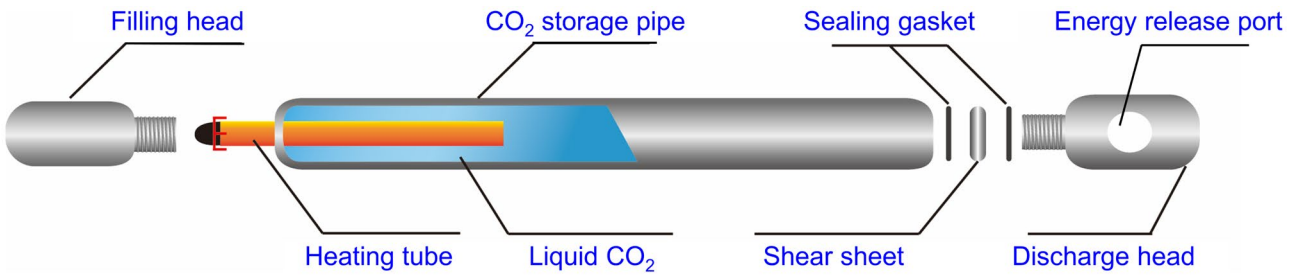

Fig. 1 Structure of carbon dioxide phase transition fracturing pipe

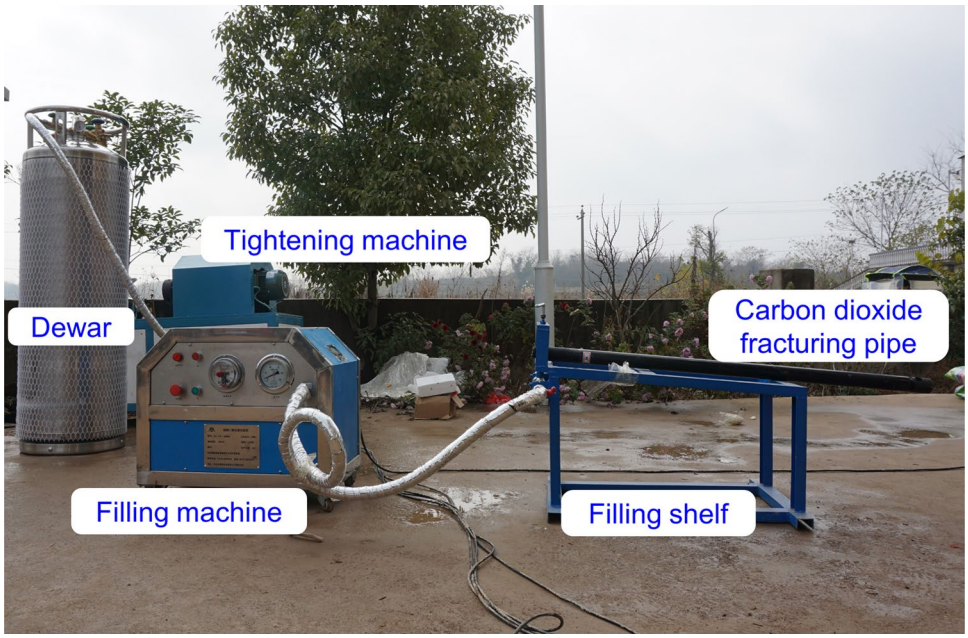

Fig. 2 Liquid carbon dioxide filling equipment

initiating device is used to energize the heating tube, and the heating tube instantly releases a large amount of heat. As the internal temperature of the storage pipe continues to increase, the inner pressure also continues to increase, and the liquid carbon dioxide is rapidly converted into the supercritical state. When the inner pressure exceeds the broken pressure of the shear sheet, the shear sheet breaks. Supercritical carbon dioxide instantly transforms into a gaseous state and it is released from the discharge head. High-pressure carbon dioxide brings extremely destructive dynamic impact in a short time, destroys the surrounding rock, and generates a certain number of impact cracks. After high-pressure gas enters the impact cracks, these cracks undergo a second propagation under the tensile stress, which

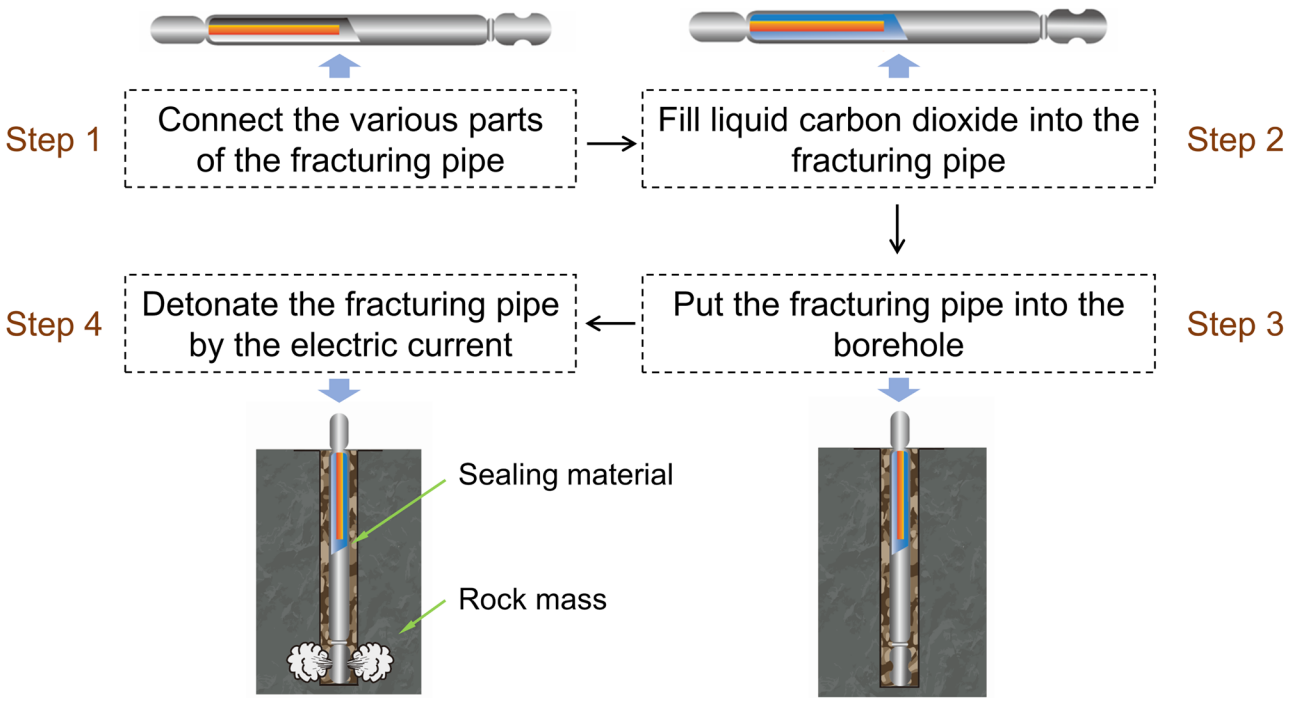

Fig. 3 Operation steps of carbon dioxide phase transition fracturing

eventually achieves the purpose of rock breaking. The operation steps of CDPTF are summarized in Fig. 3.

Single-hole carbon dioxide phase transition fracturing test

The fracturing test site we chose was located in Hubei Province, China. This test was carried on a relatively complete sandstone with no joint development. Before the in situ vibration test, the rock mass was cut to ensure that the upper free surface was flat. It had been shown in the existing research that the fracturing vibration induced by CO_2 was less than blasting vibration (Tao et al. 2018). Hence, the short hole fracturing test was chosen to make the monitoring results more significant, and the height difference between the energy release port and the ground was 0.9 m. In addition, since the volume of carbon dioxide expands by about 600 times during the fracturing process, the fracturing pipe is easily pushed out of the borehole by high-pressure CO_2 in the short hole fracturing, resulting in large vibration monitor errors. Therefore, it is essential to select the reasonable drilling diameter and the sealing materials before the short hole fracturing test. We chose 90 mm and 115 mm hole diameters, respectively, and used two different materials including a mixture of crushed stone and drill cuttings and the quick-hardening gypsum to carry out the pre-fracturing tests, as shown in Fig. 4. The results indicated that when the drill hole diameter was 90 mm, the fracturing pipe was easily pushed out of the drill hole owing to the small gas expansion space. And when we chose quick-setting gypsum, there was low strength at the bonding interface with drilling holes, and the fracturing pipe easily moved along the borehole axis. Pre-fracturing tests results indicated that only when the drill hole diameter was 115 mm and the crushed stone and drill cuttings were used to stem the drill hole, the fracturing pipe could be stable during the short hole fracturing. Therefore, such test parameters were applied to our formal vibration test.

When we conducted the vibration test, the fracturing pipe with an outer diameter of 51 mm and a length of 105 cm was used. In this test, the thickness of the shear sheet was 3.5 mm and the mass of liquid carbon dioxide in the fracturing pipe was 780 g. To investigate the influence of the gathering energy effect on the fracturing vibration, the single-hole test was chosen. TC-4850 blasting vibration testers and Micromate testers were used to collect the vibration signals in this test. Locations of vibration monitoring points were determined according to the set direction of the energy release port. A total of two columns of mutually perpendicular test points were set, and five vibration monitoring points were laid in each direction, as shown in Fig. 5. For the convenience of description, the directions for the two columns' monitoring points were named as M and S respectively. It should be explained that the jet direction of high-pressure carbon dioxide was consistent with the direction M, and the vertical jet direction is the direction S.

Attenuation law of carbon dioxide phase transition fracturing vibration

Through the above test, we have collected the vibration velocity–time curves of each monitoring point. It is indicated from the vibration monitoring results that the fracturing vibration durations in the two monitoring directions are quite short, both belong to non-stationary random signals. Although the fracturing vibration signal is a random signal like the blasting vibration, the velocity–time curve of CDPTF is smoother than that of blasting vibration, and there is no obvious high-frequency oscillation. Only one obvious peak occurs in fracturing vibration signals. As we all know, the original blasting vibration signal has multiple dense peaks in a short time. There are clear differences between these two types of vibration signals. The peak particle vibration velocities (PPVs) of fracturing vibration in the two directions are significantly different. Among them, the PPVs at point M1 and S1 in the two monitoring directions have the largest difference, and the velocity–time curves for these two monitoring points are shown in Fig. 6.

It is apparent from Fig. 6 that the durations for all three vibration components at M1 and S1 do not exceed 1 s. At the monitoring point M1, the vertical PPV is the largest, followed by transversal PPV, and the longitudinal PPV is the smallest. Different from M1, at the monitoring point S1, the longitudinal PPV is the largest, followed by the vertical PPV, and the transversal PPV is the smallest. Comparing the vibration components in the three directions of M1, the vertical vibration lasts the longest, and the duration of the remaining two vibration components is close to each other. Different from M1, the durations of the three-component vibration curves at S1 are close to the same.

To investigate the attenuation law of PPV and Fourier dominant frequency, the PPVs and Fourier dominant frequencies of all monitoring points in the jet direction (i.e., direction M) and vertical jet direction (i.e., direction S) are listed in Tables 1 and 2.

The dominant vibration direction of each monitoring point in jet direction is vertical. Different from it, the dominant vibration direction for the vertical jet direction is longitudinal. PPVs in both monitoring directions decrease with the explosion center distance increases. Affected by the gathering energy effect, the PPVs have obvious direction differences in these two directions. The PPVs in jet direction are greater than those in vertical jet direction, which is obvious in the range of 2.193–3.132 m. The reason for

(a) Stemming with reduced stones and drill cuttings

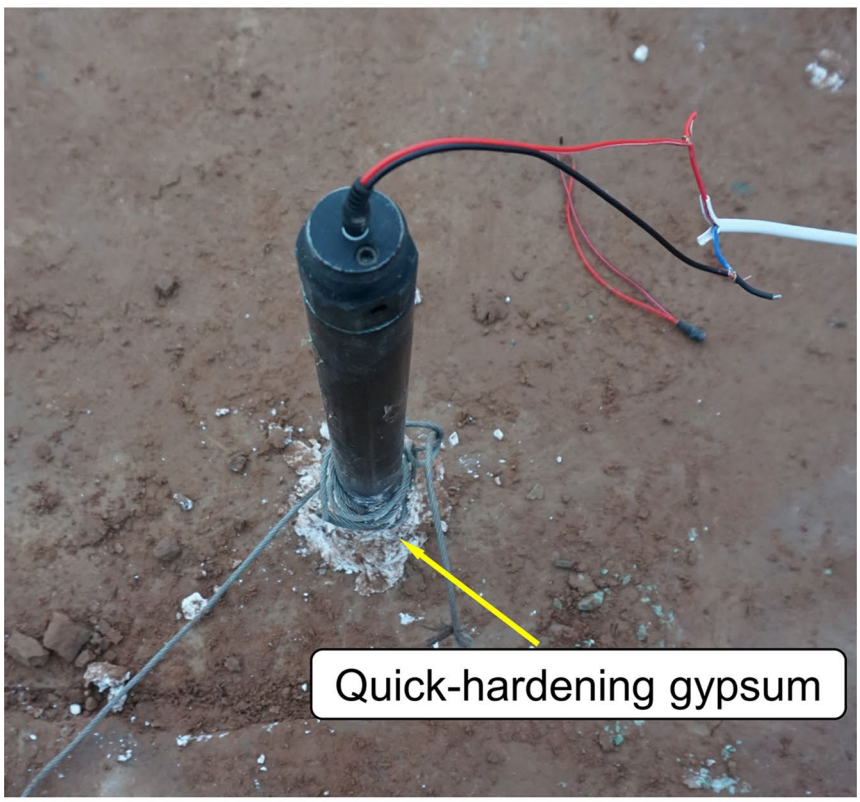

(b) Stemming with quick-hardening gypsum

Fig. 4 Stemming situations of pre-experiments. **a** Stemming with reduced stones and drill cuttings. **b** Stemming with quick-hardening gypsum

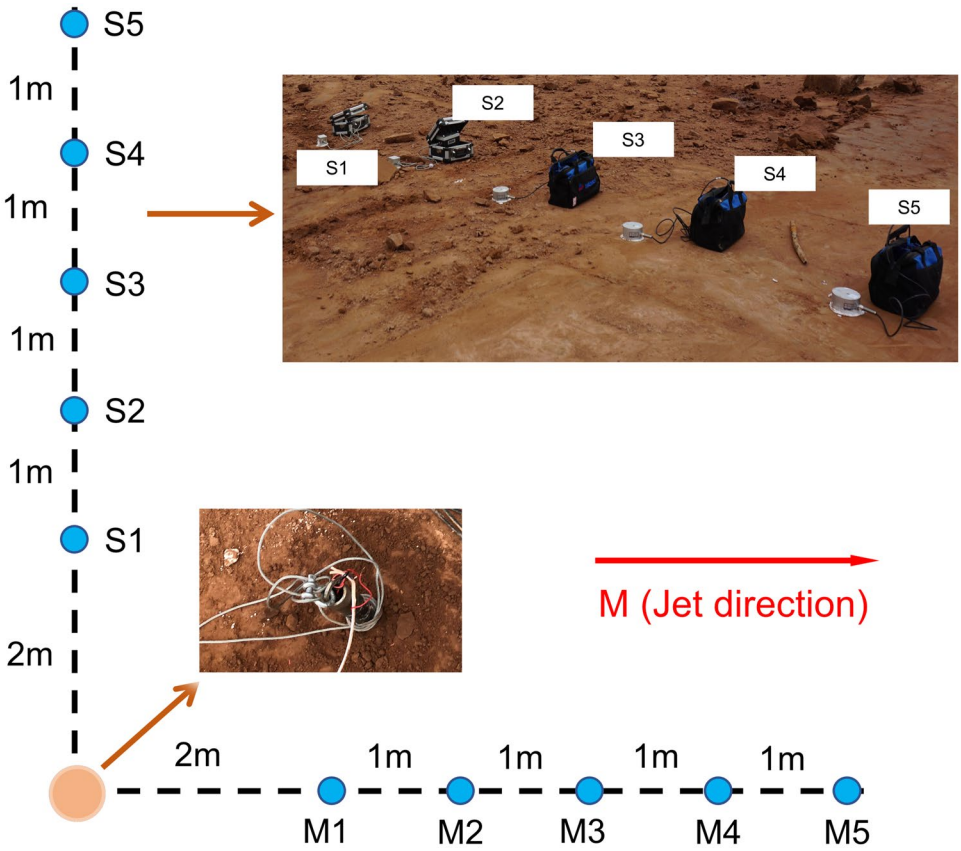

Fig. 5 Vibration monitoring points layout for the carbon dioxide phase transition fracturing test

this phenomenon is that when the high-pressure CO_2 is discharged from the energy release port, it quickly impacts the drill hole wall which faces the jet directly, and the surrounding rock mass in the jet direction is subjected to a greater impact force (Zhou et al. 2020); the corresponding stress wave is apparently larger than that of vertical jet direction. Fitting the PPV data in the two monitoring directions, the attenuation equation in jet direction is:

$$v_1 = 30.31r^{-2.342} \qquad R^2 = 0.991 \tag{1}$$

where v_1 is the peak particle velocity for the jet direction (cm/s); r is the explosion center distance, that is, the distance between the monitoring point and the explosion center (m).

The PPV attenuation equation in the vertical jet direction is:

$$v_2 = 17.50r^{-1.988} \qquad R^2 = 0.969 \tag{2}$$

where v_2 is the peak particle velocity in the vertical jet direction (cm/s).

It is generally acknowledged that, in the far field, the attenuation for stress waves and the vibration obeys the power function when we use explosives to excavate the rocks. The above Eqs. (1) and (2) indicate that the PPVs for ground vibration in both directions under the CDPTF also decay as a power function with the increasing explosion center distance. In some sensitive projects, the excavation area is very close to the building. To reduce the damage of repeated impact to the surrounding rock, single-hole presplitting fracturing under the condition of a single free surface is sometimes carried out before multiple drill hole fracturing. In this case, we could combine such fitting formula with the standard safety regulations to quickly determine the reasonable safety distance between the drill hole and the protected buildings, which is beneficial for our drilling design. It should be pointed out that the vertical vibration is often the largest in existing studies, but our test results indicate that the peak vertical vibration is largest only in jet direction. This phenomenon may be related to the layouts of fracturing pipes and monitoring points, because the existing studies are mostly carried out with multiple fracturing pipes, and monitoring points were set up only in one line. Noting that our test results do not only obey the traditional vibration propagation theory, the attenuation law is also consistent with the previous results (Chen et al. 2018; Zeng et al. 2020), which fully certifies that the monitoring results in our test for fracturing vibration are reliable.

As shown in Tables 1 and 2 and Fig. 7b, the Fourier dominant frequency for jet direction has been fluctuating slightly around 2 Hz, and it nearly does not change with the explosion center distance increases, but the dominant frequency in the vertical jet direction decreases as the

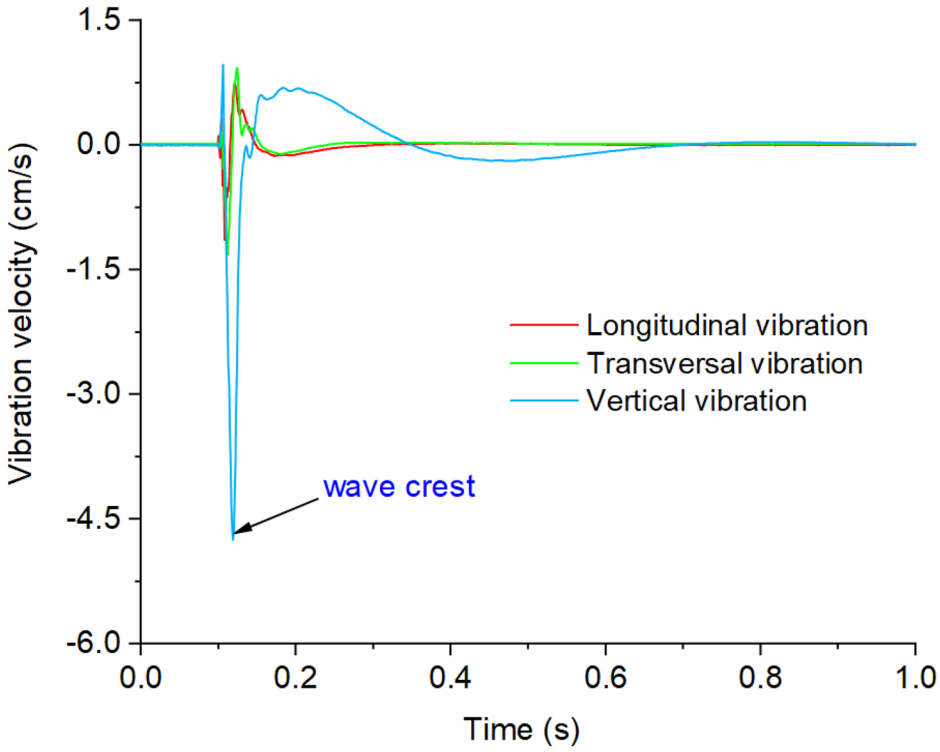

(a) Velocity-time curves of monitoring point M1

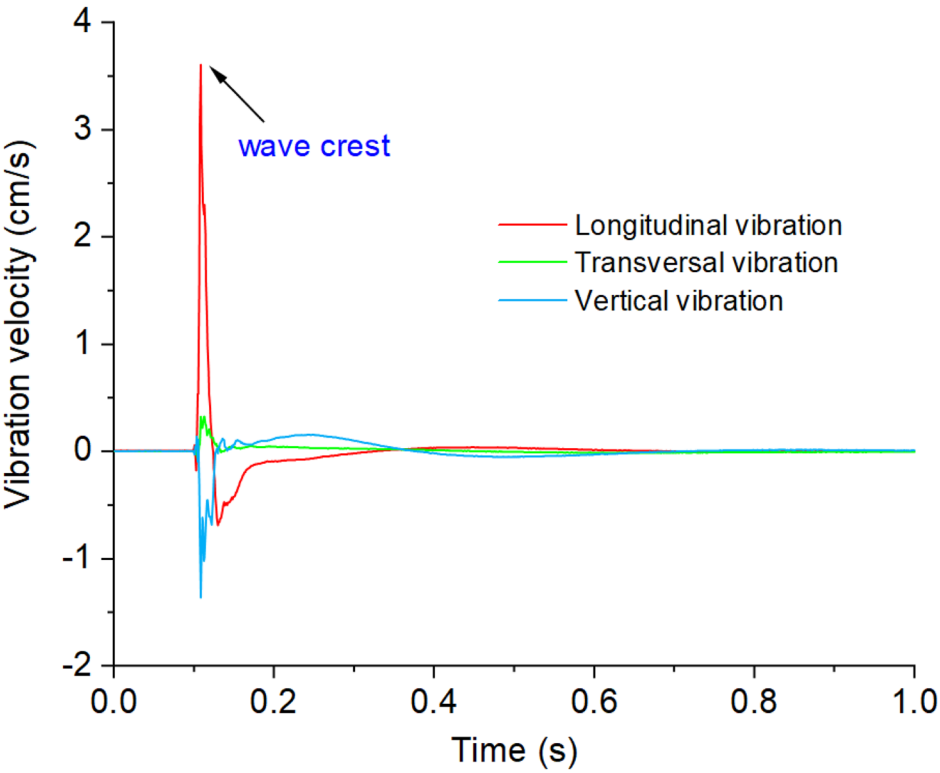

(b) Velocity-time curves of monitoring point S1

Fig. 6 Representative velocity–time curves in two different monitoring directions. **a** Velocity–time curves of monitoring point M1. **b** Velocity–time curves of monitoring point S1

Table 1 PPVs and dominant frequencies in jet direction (i.e., direction M)

Explosion center distance (m)	Dominant frequency (Hz)	Particle vibration velocity (cm/s)				PPV (cm/s)
		Resultant peak velocity	Longitudinal peak velocity	Transversal peak velocity	Vertical peak velocity	
2.193	2.3	4.796	1.147	1.326	4.756	4.756
3.132	2	2.569	0.987	0.638	2.346	2.346
4.100	2.2	1.202	0.670	0.302	1.009	1.009
5.080	2	0.652	0.272	0.141	0.619	0.619
6.067	2	0.259	0.061	0.031	0.252	0.252

explosion center distance increases. When the explosion center distance grows from 2.193 to 6.067 m, the Fourier dominant frequency in the vertical jet direction decreases from 12.5 to 1.6 Hz; the largest drop of dominant frequency occurs in the range of 3.132–6.067 m. Fitting the relationship between the dominant frequency of each monitoring point in the vertical jet direction and explosion center distance, we can obtain:

$$f_{\mathrm{vd}} = -3.39r + 21.25 \qquad R^2 = 0.89 \tag{3}$$

where f_{vd} is the Fourier dominant frequency in vertical jet direction (Hz).

In general, the dominant frequency and PPV for fracturing vibration decay quickly as the propagation distance increases. For the CDPTF, when the propagation distance is short, the dominant frequency for vertical jet direction is greater than that of the jet direction. Therefore, when we take the resonance of the protected building into account, we need to consider the direction of the gas impact and the distance between the drill hole and the protected structure.

Fracturing vibration signal analysis based on Hilbert–Huang transform

Brief introduction for Hilbert–Huang transform

It is acknowledged that typical characteristics of non-stationary signals are usually obtained through signal processing methods. As a classic signal processing method, even if the fast Fourier transform (FFT) could effectively reveal the amplitude–frequency characteristics of the signal, it still cannot accurately describe the instantaneous frequency of the signal, and it is only suitable for linear stationary signals. In order to analyze non-stationary signals accurately, the wavelet analysis theory was put forward. It is acknowledged that the wavelet transform has good localized properties in the time and frequency domain, and it has been widely used in blasting vibration signal processing. In fact, the wavelet transform is a fast Fourier transform with adjustable windows. When the wavelet transform is carried, the signal in the wavelet window must be the stationary signal, so it does not get rid of the limitations in fast Fourier transform. Besides, the signal processing results based on the wavelet transform are different if the different wavelet bases are selected. With a view to overcoming the limitations of fast Fourier transform and wavelet transform, Huang et al. (1998) proposed the Hilbert–Huang transform, which is a good method based on the time scale characteristics of the data itself. The Hilbert–Huang transform does not require a priori base, which makes the signal processing more flexible. Moreover, in this method, the localization properties were emphasized, and the high- and low-frequency errors generated in the fast Fourier transform were avoided. Therefore, it is regarded as one of the most effective methods for processing nonlinear non-stationary signals. Nowadays, this method has been successfully used in seismic wave analysis, machine failure analysis, image edge detection, and other fields (Liu and Gao 2020).

Table 2 PPVs and dominant frequencies in vertical jet direction (i.e., direction S)

Explosion center distance (m)	Dominant frequency (Hz)	Particle vibration velocity (cm/s)				PPV (cm/s)
		Resultant peak velocity	Longitudinal peak velocity	Transversal peak velocity	Vertical peak velocity	
2.193	12.5	3.868	3.606	0.324	1.363	3.606
3.132	13.4	2.015	1.942	0.224	0.523	1.942
4.100	6.67	1.313	1.312	0.044	0.026	1.312
5.080	2.4	0.561	0.560	0.050	0.050	0.560
6.067	1.6	0.134	0.126	0.040	0.033	0.126

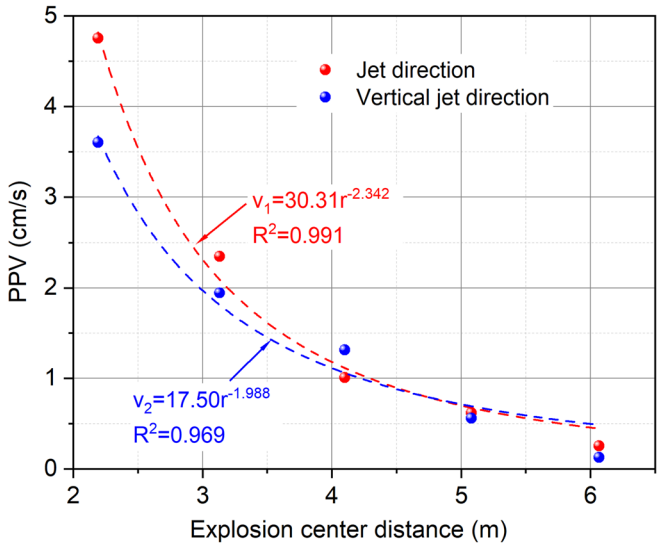

(a) Variation in peak particle velocity for two monitoring directions

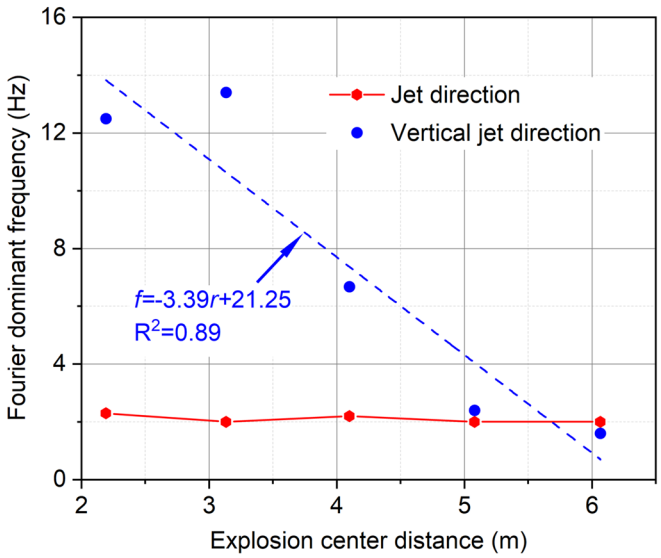

(b) Variation in Fourier dominant frequencies for two monitoring directions

Fig. 7 Variation in PPVs and Fourier dominant frequencies with the varying explosion center distance. **a** Variation in peak particle velocity for two monitoring directions. **b** Variation in Fourier dominant frequencies for two monitoring directions

The essence of the Hilbert–Huang transform is to obtain the relationship between frequency and time by smoothing the non-stationary signal. It consists of empirical mode decomposition (EMD) and the Hilbert transform. When performing the Hilbert–Huang transform, firstly, the given random unsteady signal should be adaptively decomposed into a certain sum of the eigenmode function components and a residual by the EMD:

$$v(t) = \sum_{i=1}^{n} h_i(t) + r(t) \tag{4}$$

where $v(t)$ is the original non-stationary signal, $h_i(t)$ is the ith intrinsic mode function (IMF) component, and $r(t)$ is the signal residual.

The adaptive EMD process could remove the superimposed wave and make the waveform more symmetrical. The procedures of the empirical mode decomposition are given in Fig. 8.

When the Hilbert transform is applied to the obtained IMF components, the instantaneous frequency and energy of the signal could be obtained. In addition, through synthesizing the instantaneous frequencies of all IMF components, the time–frequency–energy signal spectrum for the original signal, namely the Hilbert spectrum, can also be obtained.

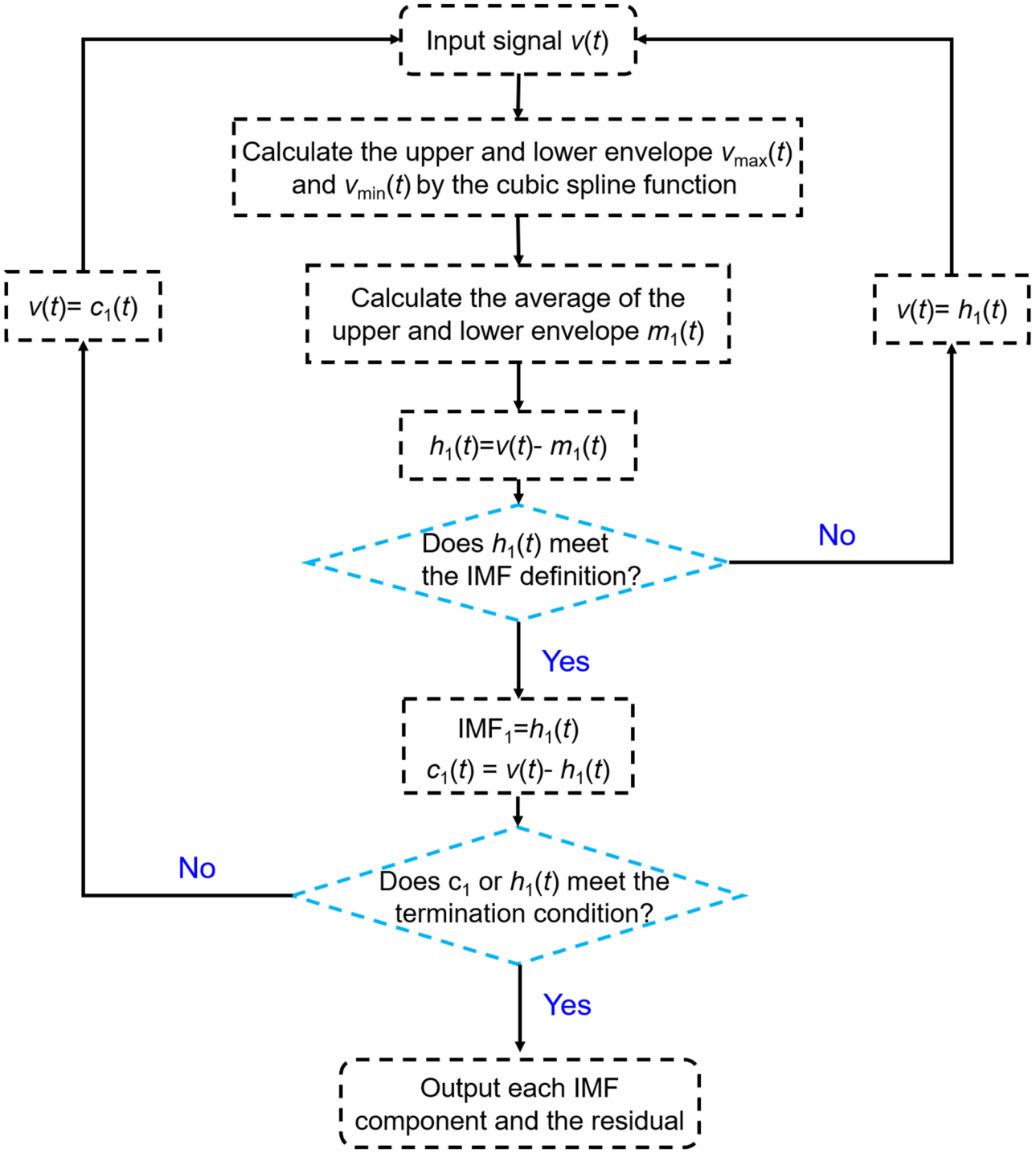

Fig. 8 Flow chart of empirical mode decomposition

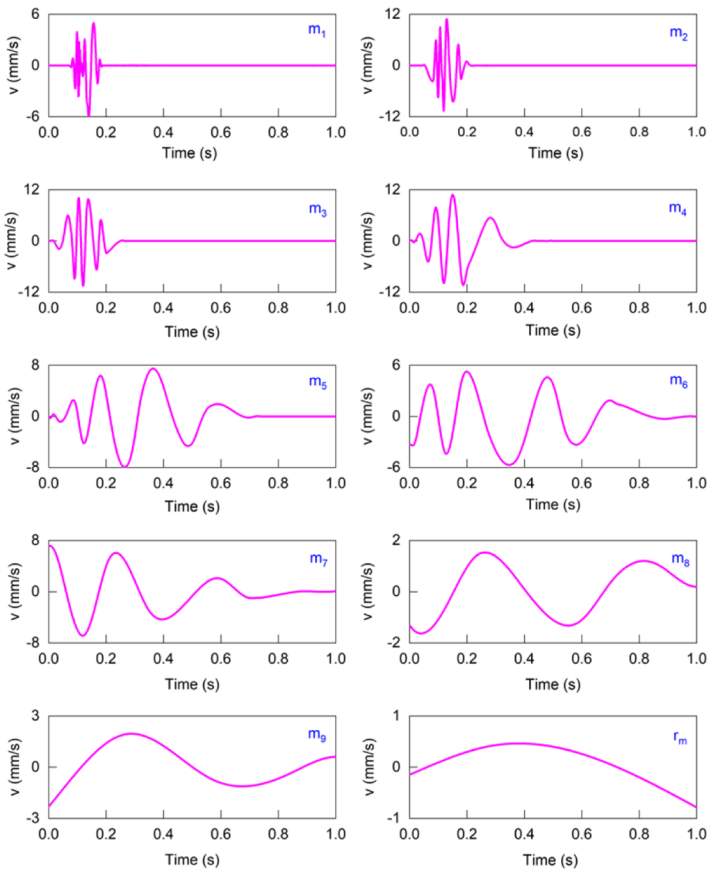

(a) IMF components and the residual of monitoring point M1

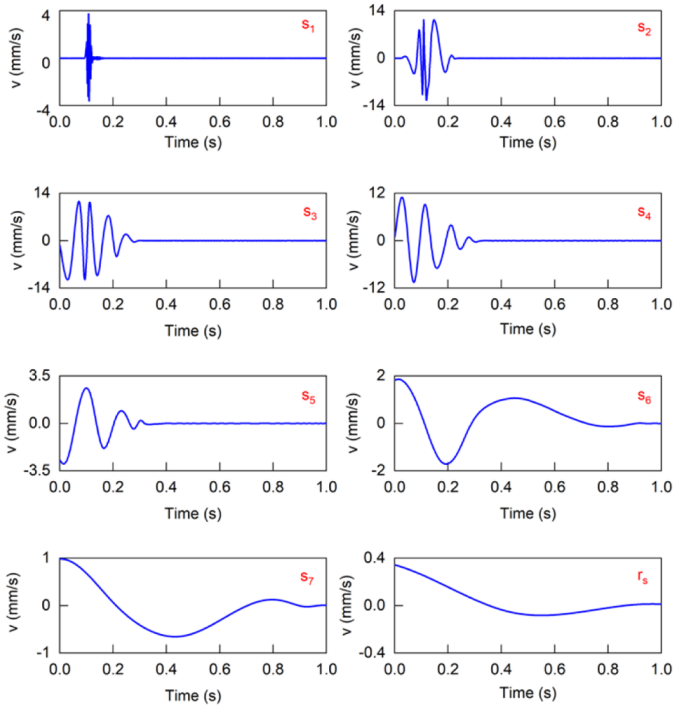

(b) IMF components and the residual of monitoring point S1

Fig. 9 IMF components and residuals of representative monitoring points M1 and S1. **a** IMF components and the residual of monitoring point M1. **b** IMF components and the residual of monitoring point S1

EMD decomposition of the fracturing vibration signal

Due to the different energy distribution ratios for the stress wave and gas wedge between the blasting and CDPTF, the vibration characteristics of CDPTF are significantly different from that of blasting vibration. With the aim to accurately get the vibration characteristics, in blasting projects, the vertical vibration curve is usually chosen as the analysis object owing to the peak value of it is always the biggest over the three monitor directions. As mentioned in the latest section, the vertical PPV for the jet direction is largest in CDPTF, and the longitudinal PPV is largest for the vertical jet direction, which is quite different from blasting vibration. According to our in situ vibration test results, the monitoring points with the largest difference in resultant PPV are M1 and S1, so the vertical velocity–time curve at M1 and the longitudinal velocity–time curve S1 were decomposed to investigate the difference between the EMD components in the two monitoring directions; the corresponding IMF components are shown in Fig. 9. Figure 10 provides the corresponding energy proportion of each IMF component.

From Figs. 9a and 10a, it is indicated that the IMF component m_1 of the vertical vibration signal at M1 has a short wavelength, high frequency, and small energy proportion, which belongs to the high-frequency noise. Among all the IMF components, m_5 has the largest energy proportion, the wavelengths of $m_2 \sim m_7$ components become longer and the frequencies decrease in sequence. These six IMF components occupy most of the signal energy, which is the dominant sub-band. Moreover, the wavelength of the $m_8 \sim m_9$ is longer than that of the $m_2 \sim m_7$ component; the frequencies and the energy proportion are both small, which might be the inherent low-frequency component. Like the m_1, the IMF component s_1 of the longitudinal vibration signal at S1 has a short wavelength, high frequency, and small energy ratio, which is the high-frequency noise of the signal. s_3 occupies the most energy in all the IMF components of the longitudinal signal. The wavelengths of the three components s_2, s_3, and s_4 become longer and the frequencies decrease in sequence; most of the energy is contained in these components. The wavelengths of $s_5 \sim s_8$ are longer than that of the $s_2 \sim s_4$ components, and the signal frequencies are lower. They are regarded as the low-frequency components of the vibration signal. Through comparing the analysis results of these two signals, we could get more information that the high-frequency noise energy at M1 accounts for a higher proportion than that of the vibration signal at S1. The number of IMF layers for the vibration signal at M1 is greater than that of the direction S1. The energy proportion of IMF components at M1 is more average.

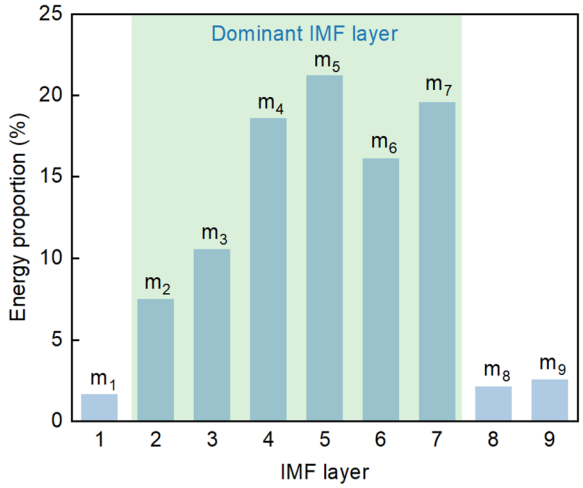

(a) Energy proportion of each IMF component at M1

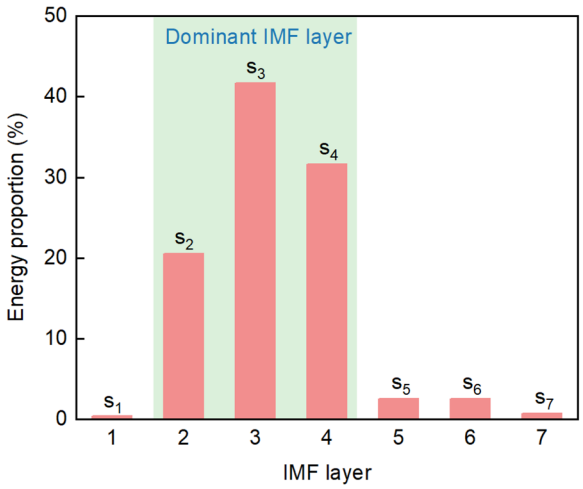

(b) Energy proportion of each IMF component at S1

Fig. 10 Energy proportion of IMF components at M1 and S1. **a** Energy proportion of each IMF component at M1. **b** Energy proportion of each IMF component at S1

Time–frequency analysis of the fracturing vibration signals in different directions

After removing all the high-frequency noise components of each monitoring curve, the Hilbert transform was applied to the IMF components corresponding to different monitoring points to obtain the HHT spectrums. The fracturing vibration signals could be further analyzed according to the obtained HHT spectrums.

As we have mentioned in the former section, the PPV of CDPTF in different directions has evident differences. It is acknowledged that the component with the highest PPV in the three vibration directions can effectively represent the vibration characteristics of the monitoring point (Zhang 2006). The dominant vibration direction in the jet direction is vertical, and the dominant vibration direction in the vertical jet direction is longitudinal. Therefore, the IMF components we have already obtained are further processed to compare the difference in time–frequency–energy characteristics of the vibration signal in the two monitoring directions. The three-dimensional time–frequency–energy spectrums of the two signals are shown in Fig. 11, and the Hilbert marginal energy spectrums are represented in Fig. 12.

The vibration signal energy at M1 is mainly distributed in 0–0.7 s, and the vibration signal at S1 is mainly distributed in 0–0.3 s, which indicates that the vibration energy at M1 is distributed in a wider time range. As can

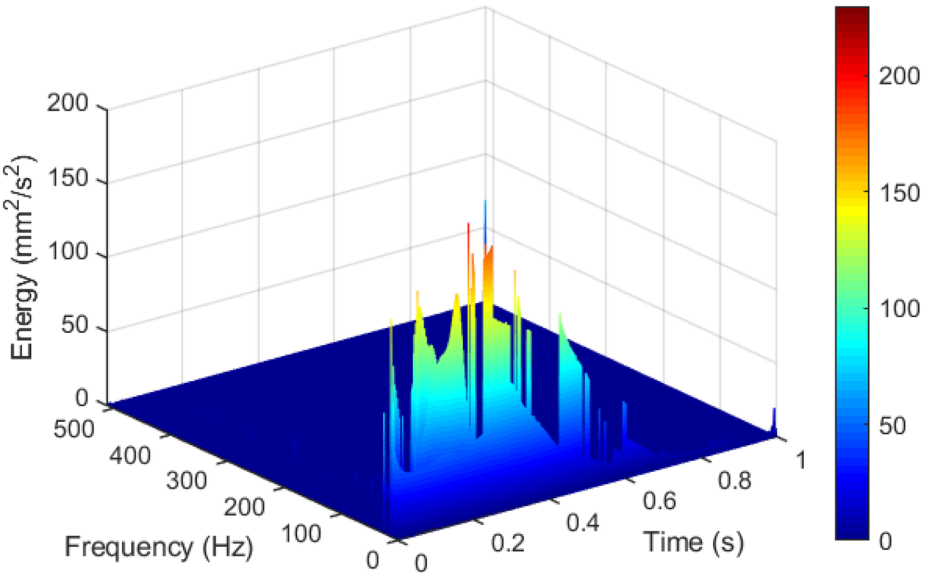

Fig. 11 Three-dimensional time–frequency energy spectrums of the dominant fracturing vibration velocity–time curves of M1 and S1. **a** Three-dimensional time–frequency energy spectrums of the fracturing vibration at M1. **b** Three-dimensional time–frequency energy spectrums of the fracturing vibration at S1

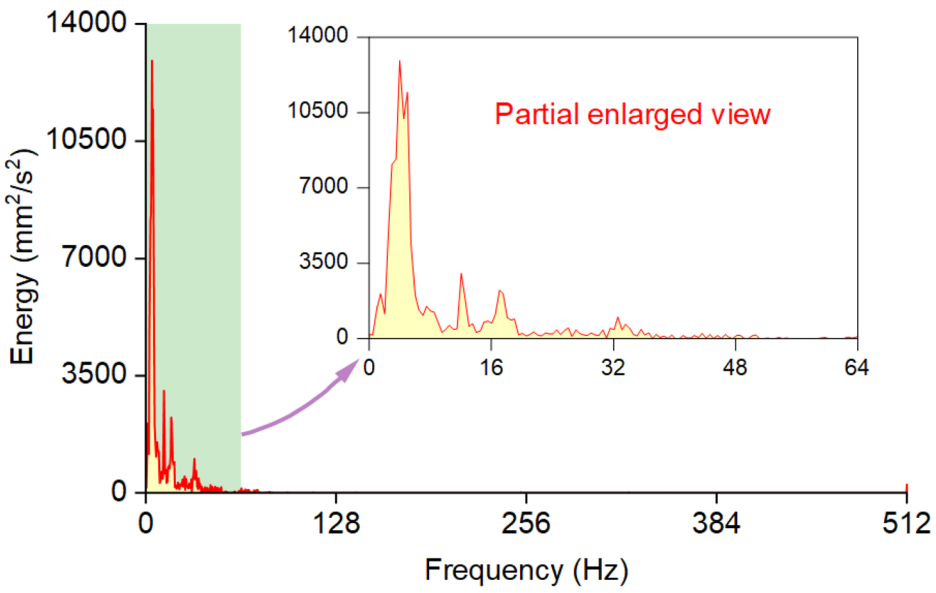

(a) Hilbert marginal energy spectrum of the vibration signal at M1

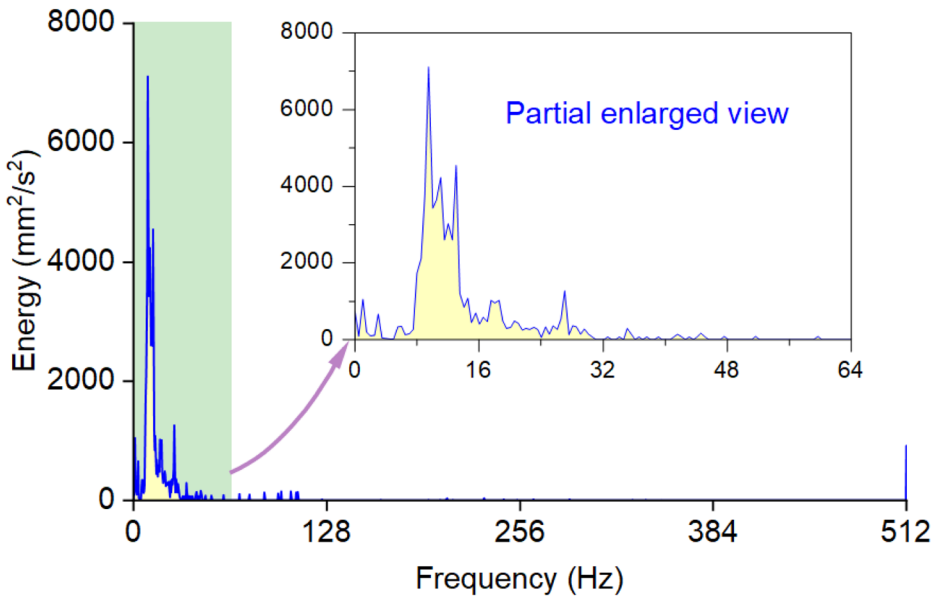

(b) Hilbert marginal energy spectrum of the vibration signal at S1

Fig. 12 Hilbert marginal energy spectrums at dominant fracturing vibration curves at M1 and S1. **a** Hilbert marginal energy spectrum of the vibration signal at M1. **b** Hilbert marginal energy spectrum of the vibration signal at S1

be seen from the Fig. 12a, b, the energies of M1 and S1 are mainly distributed within 0–48 Hz. In addition, it is also indicated from Fig. 12 that the corresponding frequency to peak energy value at S1 is higher than that of M1, which is consistent with what the Fourier dominant frequency showed. The energy distribution of M1 is more concentrated, and the main frequency range of the signal energy at M1 is in a lower frequency band than that of S1.

Vibration signal energy analysis at different explosion center distance

To investigate the energy proportion change law for the CDPTF vibration energy in each frequency band with explosion center distance changes, the HHT method was taken to evaluate the dominant vibration features of each monitoring point in the two directions. The Hilbert

Table 3 Vibration energy proportion distribution of carbon dioxide phase transition fracturing at different explosion center distance

Monitoring direction	Explosion center distance (m)	Energy proportion (%)				
		0–20 Hz	20–50 Hz	50–100 Hz	100–200 Hz	> 200 Hz
Jet direction (direction M)	2.193	87.23	11.04	1.5	0.04	1.83
	3.132	83.63	13.66	1.49	0.1	1.11
	4.100	91.79	6.87	0.61	0.26	0.47
	5.080	93.14	6.21	0.01	0	0.64
	6.067	96.40	1.35	0.16	0.03	2.06
Vertical jet direction (direction S)	2.193	83.68	13.31	1.25	0.75	1.01
	3.132	72.93	23.74	2.14	0.91	0.28
	4.100	99.07	0.72	0.09	0.05	0.07
	5.080	97.36	1.01	0.06	0.04	1.53
	6.067	94.23	2.0	0.23	0.38	2.64

marginal energy spectrums for all monitoring points were obtained. Finally, the Hilbert marginal energy spectrums in the frequency domain of 0–20 Hz, 20–50 Hz, 50–100 Hz, 100–200 Hz, and 200–512 Hz respectively were integrated to attain the vibration energy proportion in different frequency domains, as shown in Table 3.

From Table 3, we can see that the energy proportion for 0–20 Hz occupied the most energy. With the explosion center distance increases, the energy proportion of 0–20 Hz in the jet direction increases from 87.23 to 96.40%, showing an overall upward trend. With the increasing explosion center distance from 2.193 to 6.067 m, the energy proportion of the vertical direction in 0–20 Hz grows from 83.68 to 94.23%, but the growth trend is not significant. It should be noted that the energy proportion in 0–20 Hz of the vertical jet direction slightly decreased within the range of 4.100 ~ 6.067 m. What caused it might be that the fracturing vibration signal is a typical random signal with a certain random error, and the vibration curves may also be influenced by the inherent end effect in the HHT method, resulting in a small amount of energy appearing in the high-frequency band and bringing some errors. It is worth mentioning that the errors caused by this end effect also reflected in the HHT spectrum, which is specifically manifested by an energy burst near the frequency of 512 Hz. Moreover, with the increasing explosion center distance, the energy in both directions generally transforms from high frequency to low frequency. The variation of the energy proportion in 0–20 Hz with the increasing explosion center distance is shown in Fig. 13.

Since the energy proportion in 0–20 Hz of the jet direction is obviously related to the explosion center distance, fitting the energy proportion data corresponding to each monitoring point, the fitting formula can be expressed as:

$$P_E = 2.88r + 78.59 \; R^2 = 0.77 \tag{5}$$

where P_E is the energy proportion of 0–20 Hz in jet direction (%); r is the explosion center distance (m).

Discussion

Since the vibration dominant frequency of CDPTF is low, the fracturing vibration may bring resonance risk to the protected buildings (Zeng et al. 2020). Over the past few years, the ground vibration characteristics of CDPTF became an important issue that many scholars paid attention to. Several multiple drill hole fracturing vibration tests were carried out, and some beneficial results were obtained. However, these tests all ignore the effect of the gas impact direction on vibration. This issue deserves further attention because it is important for the safety control of the surrounding buildings near the fracturing area. To obtain the vibration signals of different

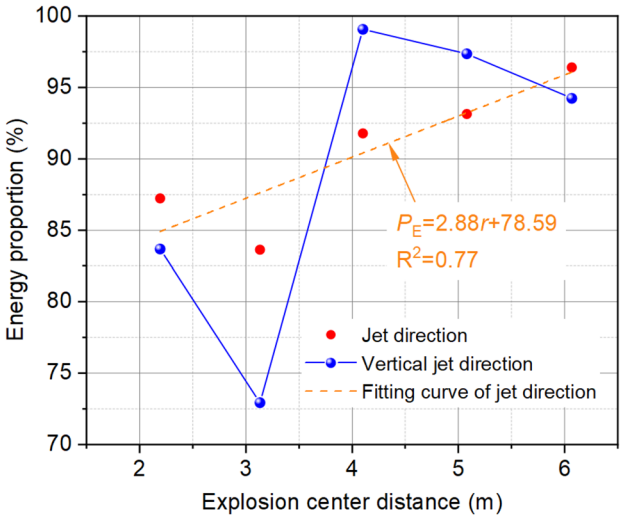

Fig. 13 Variation of the energy proportion in 0–20 Hz with the varying explosion center distance

directions, we carried out the short hole fracturing vibration test with one fracturing pipe. The signals were further processed by the HHT method to analyze time–frequency–energy characteristics. On the one hand, we found that PPV in jet direction is larger than that of vertical jet direction. Moreover, in jet direction, the peak vertical velocity is the largest of the three velocity components at the same monitoring point. On the other hand, the test results indicate that the dominant frequency in jet direction does not change with the increasing explosion center distance, but it decays in vertical jet direction. When the resonance of the protected structure needs to be considered, the borehole–building distance and the CO_2 jet direction should be determined according to the attenuation fitting equations of PPV and dominant frequency in different directions.

It should be noted that, in others' fracturing tests, the peak vertical velocity is almost the largest. This difference may be related to the numbers and installation direction of fracturing pipes and the arrangement of monitoring points. The existing studies did not consider the directionality of gas impact. In fact, the test in this paper also has its limitations. Limited by the test site conditions, we only collected the ground vibration signals under a single free surface in this study, and the test results of more free surfaces like bench fracturing were not obtained. In addition, due to the limitation of testing sensor numbers, we only monitored the vibration in two directions. We can imagine that if we set up monitoring points in more directions, we would get the change laws of the PPV and dominant frequency in the entire monitoring plane. When we established the regression equation of PPV, the explosion center distance was the only parameters we considered. As mentioned earlier, if we get the PPVs of more directions in the monitoring plane, we can establish a more advanced equation between the explosion center distance, the angle between the monitoring direction and the jet direction, and the peak particle velocity. Based on these issues, further vibration tests should be carried out in the future.

Conclusions

This study set out to investigate the vibration difference in different directions for CDPTF. A single short-hole carbon dioxide phase transition fracturing vibration test was carried out, and the vibration signals of CDPTF in the jet direction and the vertical jet direction was attained. Based on the monitoring data, this paper has investigated three questions, including the attenuation laws of the PPV and the Fourier dominant frequency in two monitoring directions, time–frequency characteristics for the monitoring signals, and energy distribution of the vibration signals in jet direction and vertical jet direction. The following conclusions can be drawn:

1. The vibration signal for CDPTF is a kind of random non-stationary signal with no obvious high-frequency oscillation. Dominant vibration directions of monitoring points in jet direction and vertical jet direction are the vertical direction and the longitudinal direction respectively. In addition, one of the significant findings to emerge from this study is that the PPV in jet direction is generally greater than that of the vertical jet direction. Regression analysis reveals that the PPVs of jet direction and vertical jet direction decay in a power function in the monitoring range with the increasing explosion center distance.
2. When the explosion center distance increases from 2.193 to 6.067 m, the Fourier dominant frequency decays from 12.5 to 1.6 Hz in the vertical jet direction; this attenuation satisfies the linear attenuation equation. But different test result occurred in jet direction, explosion center distance makes no significant difference to the Fourier dominant frequency, and the Fourier dominant frequency slightly fluctuates around 2 Hz in this direction.
3. The vibration signal energy in jet direction and vertical jet direction were both distributed within 0–48 Hz. With the explosion center distance increases from 2.193 to 6.067 m, the energy proportion of 0–20 Hz in the jet direction grows from 87.23 to 96.40%, and it showed a linear growth trend. It is noted that under the same condition, the energy proportion of the vertical direction in 0–20 Hz increases from 83.68 to 94.23%, but the law of growth is not significant. It is also indicated that the vibration energy converses from high frequency to low frequency as the explosion center distance rises.
4. These new findings above should help to improve understanding of fracturing vibration. When taking building safety into account, the drilling design should not only consider the safety distance, but also the installation direction of the fracturing pipe. In the future, more tests need to be carried out to refine the drilling design method and meet the requirements for safety control.

Acknowledgements This project was supported by the National Natural Science Foundation of China (42072309, 41807265) and the Hubei Key Laboratory of Blasting Engineering Foundation (HKLBEF202002). All authors appreciate the scholars from Hubei (Wuhan) Institute of Explosion and Blasting Technology and Hubei Key Laboratory of Blasting Engineering for the technical support provided in the in situ vibration test. They are Prof. Yingkang Yao, Prof. Jinshan Sun, and Mr. Xiaowu Huang. Special thanks are given to the two anonymous reviewers who have helped to improve the paper.

References

Caldwell T (2005) A comparison of non-explosive rock breaking techniques. In: Proceedings of the 12th Australian Tunnelling Conference 2005: Tunnelling Towards Better Cities. Australian Underground Construction and Tunnelling Association, p 77

Cao Y, Zhang J, Zhai H, Fu G, Tian L, Liu S (2017) CO_2 gas fracturing: a novel reservoir stimulation technology in low permeability gassy coal seams. Fuel 203:197–207

Chen G, Li Q, Liu X, Wu Z, Ma J (2018) Research on energy distribution characters about liquid CO_2 phase-transition broken rock vibration signal. Blasting 35(02):155–163 (in Chinese)

Chen H, Wang Z, Chen X, Chen X, Wang L (2017a) Increasing permeability of coal seams using the phase energy of liquid carbon dioxide. J CO2 Util 19:112–119

Chen H, Wang Z, Qi L, An F (2017b) Effect of liquid carbon dioxide phase transition fracturing technology on gas drainage. Arab J Geosci 10(14):314

Chen Y, Zhang H, Zhu Z, Ren T, Cao C, Zhu F, Li Y (2019) A new shock-wave test apparatus for liquid CO_2 blasting and measurement analysis. Meas Control 52(5–6):399–408

Clairet J (1952) Use of Cardox in coal mining in Sarre. Revue del 'Industrie Minerale 33:846–854

Dong Q, Wang Z, Han Y, Sun X (2014) Research on TNT equivalent of liquid CO_2 phase-transition fracturing. China Saf Sci J 24(11):84–88 (in Chinese)

Gao F, Tang L, Zhou K, Zhang Y, Ke B (2018) Mechanism analysis of liquid carbon dioxide phase transition for fracturing rock masses. Energies 11(11):2909

Guo Y (2017) Fracturing mechanisms and functions of improvement of gas drainage of highly pressurized carbon dioxide gas system. Master's thesis, Henan Polytechnic University, Jiaozuo, China (in Chinese)

Guo Y, Ke B, Wu Z, Ren G (2018) Thermodynamic properties of liquid carbon dioxide blasting system in process of phase transformation. Blasting 35(04):108–115 (in Chinese)

Hawkes I (1958) The blasting action of the Cardox shell. Trans Inst Min Eng 118(1)

He W, He F, Zhang K, Zhao Y, Zhu H (2018) Increasing permeability of coal seam and improving gas drainage using a liquid carbon dioxide phase transition explosive technology. Adv Civ Eng 3976505

Hu S, Pang S, Yan Z (2019) A new dynamic fracturing method: deflagration fracturing technology with carbon dioxide. Int J Fract 220(1):99–111

Huang NE, Shen Z, Long SR, Wu MC, Shih HH, Zheng Q, Yen N, Tung CC, Liu HH (1998) The empirical mode decomposition and the Hilbert spectrum for nonlinear and non-stationary time series analysis. Proc Math Phys Eng Sci 454:903–995

Jiang N, Zhu B, He X, Zhou C, Luo X, Wu T (2020) Safety assessment of buried pressurized gas pipelines subject to blasting vibrations induced by metro foundation pit excavation. Tunn Undergr Space Technol 102:103448

Kang J, Zhou F, Qiang Z, Zhu S (2018) Evaluation of gas drainage and coal permeability improvement with liquid CO_2 gasification blasting. Adv Mech Eng 10(4):168781401876857

Ke B, Zhou K, Li J, Zhang Y, Shi W, Cheng L, Yang J (2017) Time-frequency analysis of seismic wave for liquid CO_2 blasting system. Blasting 34(04):137–142+148 (in Chinese)

Ke B, Zhou K, Xu C, Ren G, Jiang T (2019a) Thermodynamic properties and explosion energy analysis of carbon dioxide blasting systems. Min Technol 128(1):39–50

Ke B, Zhou K, Ren G, Shi J, Zhang Y (2019b) Positive phase pressure function and pressure attenuation characteristic of a liquid carbon dioxide blasting system. Energies 12(21):4134

Li Q, Chen G, Luo D, Ma H, Liu Y (2020) An experimental study of a novel liquid carbon dioxide rock-breaking technology. Int J Rock Mech Min 128:104244

Liu X, Wang Z, Song D, He X, Yang T (2020) Variations in surface fractal characteristics of coal subjected to liquid CO_2 phase transition fracturing. Int J Energy Res. https://doi.org/10.1002/er.5568

Liu J, Gao W (2020) Vibration signal analysis of water seal blasting based on wavelet threshold denoising and HHT transformation. Adv Civ Eng 4381480

Liu X, Li Q, Feng G, Chen G, Xie X (2018) Vibrational energy distribution of rock broken by phase transition of liquid carbon dioxide. Min Eng 38(03):5–10 (in Chinese)

Lu T, Wang Z, Yang H, Yuan P, Han Y, Sun X (2015) Improvement of coal seam gas drainage by underpanel cross-strata stimulation using highly pressurized gas. Int J Rock Mech Min Sci 77:300–312

Miller RCI (1995) Fundamental study of carbon dioxide blasting: an experimental and numerical analysis of surface cleaning by a particle-laden turbulent jet

Ozer U (2008) Environmental impacts of ground vibration induced by blasting at different rock units on the Kadikoy-Kartal metro tunnel. Eng Geol 100(1–2):82–90

Pantovic R, Milic V, Stojadinovic S (2002) Consideration of possibilities for application of CARDOX method in purpose of improvement of coal fragmentation. In: IOC 2002: 34th International October Conference on Mining and Metallurgy, pp 131–135

Patrick V (1995) CO_2 blasting in Europe. Nucl Eng Int 45

Singh SP (1998) Non-explosive applications of the PCF concept for underground excavation. Tunn Undergr Space Technol 13(3):305–311

Tao M, Zhao H, Li X, Ma A (2018) Comprehensive comparative analysis of liquid CO_2 phase transition fracturing and explosive rock fracturing. Blasting 35(02):41–49 (in Chinese)

Vidanovic N, Ognjanovic S, Ilincic N, Ilic N, Tokalic R (2011) Application of unconventional methods of underground premises construction in coal mines. Tech Technol Educ Ma 6(4):861–865

Weir P, Edwards JH (1928) Mechanical loading and Cardox revolutionize an old mine. Coal Age 33:288–290

Wilson HH (1954) Coal augers: development and application underground. Trans Inst Min Eng 113:524–539

Xu J, Zhai C, Qin L, Yu G (2017) Evaluation research of the fracturing capacity of non-explosive expansion material applied to coal-seam roof rock. Int J Rock Mech Min Sci 94:103–111

Yang C, Hu J, Ma S (2019a) Numerical investigation of rock breaking mechanism with supercritical carbon dioxide jet by SPH-FEM approach. IEEE Access 7:55485–55495

Yang X, Wen G, Sun H, Li X, Lu T, Dai L, Cao J, Li L (2019b) Environmentally friendly techniques for high gas content thick coal seam stimulation-multi-discharge CO_2 fracturing system. J Nat Gas Sci Eng 61:71–82

Yang X, Wen G, Lu T, Wang B, Li X, Cao J, Lv G, Yuan G (2019c) Optimization and field application of CO_2 gas fracturing technique for enhancing CBM extraction. Nat Resour Res 29(3):1875–1896

Zeng Y, Li H, Xia X, Deng S, Zuo H, Yue H, Luo H (2020) Research on time-frequency characteristics for blasting vibration signal of CO_2 blasting by frequency slice wavelet transform. Eng Lett 28(4)

Zhang W, Zhang D, Wang H, Cheng J (2015) Comprehensive technical support for high-quality anthracite production: a case study in the Xinqiao coal mine, Yongxia mining Area. China Minerals 5(4):919–935

Zhang Y (2006) HHT analysis of blasting vibration and its application. Ph.D. thesis, Central South University, Changsha, China (in Chinese)

Zhang Y, Deng J, Deng H, Ke B (2019) Peridynamics simulation of rock fracturing under liquid carbon dioxide blasting. Int J Damage Mech 28(7):1038–1052

Zhang Y, Deng J, Ke B, Deng H, Li J (2018) Experimental study on explosion pressure and rock breaking characteristics under liquid carbon dioxide blasting. Adv Civ Eng 7840125

Zhang Y, Li E, Liu J, Leng X, Li W (2013) Applications of carbon dioxide cannon blasting on the problem of triangular flap top in coal mine handling mechanized mining face. Appl Mech Mater 256:71–74

Zhou S, Jiang N, He X, Luo X (2020) Rock breaking and dynamic response characteristics of carbon dioxide phase transition fracturing considering the gathering energy effect. Energies 13(6):1336

Zou DH, Panawalage S (2001) Passive and triggered explosion barriers in underground coal mines-A literature review of recent research. CANMET Natural Resources Canada